Journal of Materials Chemistry C

PAPER

View Article Online
View Journal | View Issue

Cite this: J. Mater. Chem. C, 2015, 3, 10309

Unusual structural-disorder stability of mechanochemically derived-$Pb(Sc_{0.5}Nb_{0.5})O_3$†

Hana Uršič,*[a] Andreja Benčan,[a] Goran Dražič,[ab] Giovanni Esteves,[c] Jacob L. Jones,[c] Tedi-Marie Usher,[c] Tadej Rojac,[a] Silvo Drnovšek,[a] Marco Deluca,[de] Jenny Jouin,[f] Vid Bobnar,[a] Gregor Trefalt,‡[a] Janez Holc[a] and Barbara Malič[a]

Received 20th July 2015,
Accepted 9th September 2015

DOI: 10.1039/c5tc02205c

www.rsc.org/MaterialsC

This study demonstrates the important effect of processing on the B-site ordering in $Pb(Sc_{0.5}Nb_{0.5})O_3$ ceramics. In contradiction to previous observations on ceramics prepared from solid state synthesis powders, which show a distinctive B-site cation ordering when annealed below ~1200 °C, in mechanochemically derived ceramics sintered 200 °C below this temperature, we do not observe such ordering, regardless of the conditions of thermal post-annealing. Accordingly, atomic-scale transmission electron microscopy revealed nanometer-sized B-site ordered regions in mechanochemically derived ceramics contrary to the larger regions extending through the whole grains in solid-state derived ceramics.

Introduction

B-site cation ordering has been used to engineer new perovskite materials and has a profound effect on the properties of different perovskites. For example, it can influence the magneto-transport properties or enhance the multiferroic properties of some perovskite materials.[1,2] In $Pb(Sc_{0.5}Nb_{0.5})O_3$ (PSN), which is a $Pb(B_{0.5}'B_{0.5}'')O_3$ type perovskite, ordering or disordering of the B-site cations, Sc^{3+} and Nb^{5+} (referred to as the ordering or disordering in further text) exhibits a strong effect on the dielectric and ferroelectric properties as well as the diffusive phase transition behaviour.[3–5] PSN can exist in the disordered state where the B′ and B″ cations are randomly distributed on the B-sites of the perovskite lattice, or in the long-range ordered state where the B′ and B″ atoms alternatively occupy the B-sites along the [111] direction of the rhombohedral cell. In the ordered state, each type of B-cation is located in its own sublattice, thus creating a superstructure with complete translational symmetry. Hence, the ordering is evidenced by the presence of superstructure peaks in X-ray diffraction (XRD) patterns with the reflection corresponding to the $(\frac{1}{2}\frac{1}{2}\frac{1}{2})$ supercell being the most pronounced.[5–7]

Ordering or disordering of B-site cations in PSN is traditionally achieved *via* annealing, respectively, below or above the order–disorder transition (T_{OD}), which is at ~1200 °C.[3,4] The reported preparation conditions for disordered and ordered PSN ceramics are summarized in ESI,† Table S1. Note that all previously reported PSN ceramics were prepared by solid-state synthesis. The disordered PSN was obtained by annealing at temperatures above the order–disorder transition.[3,5,6,8–10] In contrast, the ceramics with a high ordering degree, *i.e.*, the ordered ceramics, were annealed between 940 and 1000 °C, for at least 2 h or as long as 1 month.[3,5,6,9–11] Note here that even if the ceramic is B-site disordered after sintering, it becomes B-site ordered once it is post-annealed at 1000 °C.[6,9,11] Curiously, this order–disorder transition is even more complex in PSN single crystals. Here, the crystallization conditions have been shown to significantly affect the ordering of B-site cations; for example, by increasing the crystallization temperature toward T_{OD}, a progressive transition to the disordered state was observed; however, if the crystallization temperature was much lower (~300 °C) than T_{OD}, the crystals showed the characteristics of B-site disordering.[12]

Obtaining single-phase PSN ceramics from constituent oxides using conventional solid-state synthesis has been difficult in the past.[3,4] Attempts to prepare dense, single-phase PSN ceramics have usually involved the two-step 'columbite' method, which includes the homogenization of the B-site cations in the first step followed by another calcination of the B-oxides with the lead oxide.[13] This method usually yielded a single-phase material,[5,6,8–10] however, not all attempts were successful.[9,14]

In this work, the mixture of constituent metal oxide powders was mechanochemically activated (further referred to as "MA"), *i.e.* high-energy milled. Synthesizing the material *via*

[a] Jožef Stefan Institute, Jamova cesta 39, Ljubljana, Slovenia. E-mail: hana.ursic@ijs.si; Fax: +386 1 477 38 87; Tel: +386 1 477 3936
[b] Laboratory for Materials Chemistry, National Institute of Chemistry, Ljubljana, Slovenia
[c] Department of Materials Science and Engineering, North Carolina State University, Raleigh, NC, USA
[d] Institut für Struktur- und Funktionskeramik, Montanuniversitaet Leoben, Peter Tunner Str. 5, Leoben, Austria
[e] Materials Center Leoben Forschung GmbH, Roseggerstr. 12, Leoben, Austria
[f] Science des Procédés Céramiques et de Traitements de Surface, Centre Européen de la Céramique, 12 rue Atlantis, Limoges Cedex, France

† Electronic supplementary information (ESI) available: Experimental methods, characterization and additional figures and tables. See DOI: 10.1039/c5tc02205c

‡ Current address: University of Geneva, Switzerland.

mechanochemical activation allows for increased reactivity and PSN powders with a high degree of chemical homogeneity can be produced with one calcination step. Mechanochemically synthesized or activated powders have been previously used for the preparation of several other lead-based relaxor-ferroelectric ceramics, including $Pb(Mg_{0.33}Nb_{0.66})O_3$ (PMN),[15,16] $Pb(Sc_{0.5}Ta_{0.5})O_3$ (PST),[17] $Pb(Mg_{0.33}Nb_{0.66})O_3$–$PbTiO_3$ (PMN–PT),[18–21] $Pb(Sc_{0.5}Nb_{0.5})O_3$–$PbTiO_3$ (PSN–PT)[22,23] and $Pb(Zn_{0.33}Nb_{0.66})O_3$–$PbTiO_3$ (PZN–PT).[24] Compared with the classical solid-state synthesis, the ceramics prepared from the MA powders have exhibited superior chemical homogeneity. High chemical homogeneity of the B-site cations was shown for the MA-derived $(K_{0.485}Na_{0.485}Li_{0.03})(Nb_{0.8}Ta_{0.2})O_3$ ceramics.[25] Furthermore in PST, the B-site ordering was hindered by processing the powders by MA.[17] Since the ordering process in the PSN material depends on the diffusion of the B-site cations, it is possible that the mechanochemically derived PSN ceramics might exhibit different order/disorder behaviour compared to the PSN ceramics reported so far.

In this paper, we provide evidence for the first time that B-site ordering in the PSN ceramics and related functional properties depend on the synthesis method. Namely, in PSN ceramics prepared from MA powder B-site cation disorder was observed in the ceramics sintered ~200 °C below T_{OD} regardless the conditions of thermal post-annealing. These results contrast those on PSN ceramics prepared *via* solid-state synthesis, where the order–disorder transition was clearly observed at ~1200 °C, in agreement with the existing literature.

Experimental

For the synthesis of the PSN powders, PbO (99.9%, Sigma-Aldrich, 211907), Sc_2O_3 (99.9% Alfa Aesar, 11216) and Nb_2O_5 (99.9%, Sigma-Aldrich, 208515) were used. The homogenized, stoichiometric mixture (200 g) was MA in a high-energy planetary mill (Retsch, Model PM 400) for 24 h at 300 rpm using 15 WC balls ($2r$ = 20 mm) in a 250 ml WC vial. The powder was then heated in a closed alumina crucible at 800 °C for 1 h. The XRD patterns of the powders after mechanochemical activation and after heating were recorded (ESI,† Fig. S1) using a PANalytical X'Pert PRO MPD (PANalytical, Almelo, Netherlands) diffractometer with $CuK_{\alpha 1}$ radiation (λ = 1.54056 Å) in the 2θ-region from 10° to 70° using a detector with a capture angle of 2.122°. The exposure time for each step was 100 s and the interval between the obtained data points was 0.034°. The XRD pattern of the heated powder evidences a well crystallized perovskite phase and no traces of secondary phases, such as pyrochlore or PbO. The synthesized powder was milled in an attrition mill with yttria-stabilized zirconia (YSZ) balls in isopropanol at 800 min^{-1} for 4 h to achieve de-agglomeration, as reported previously for PMN–PT[21] and PSN–PT.[22] The particle size distribution, determined from the area distribution, was measured by laser granulometry (Microtrac S 3500), which is shown in ESI,† Fig. S2. The powder was uniform, consisting of particles with size around a few hundreds of nm. The powder compacts were prepared by isostatic pressing at 300 MPa and sintered in double alumina crucibles within packing powder with the same chemical composition as the compact to avoid possible PbO losses. In the study of the ordering effect, different thermal treatments of the PSN powder compacts were employed, as shown in Table 1. The *MA1420q* ceramics were heated above T_{OD}, while other samples were exposed to lower temperatures. The densities of the sintered pellets were determined using Archimedes' method in water at 25 °C.

Table 1 Thermal treatment conditions of the PSN ceramics prepared from the mechanochemically activated (MA) and solid-state (SS) derived powders. In all experiments the samples were heated in the presence of the packing powder

Thermal treatment	Short name
1420 °C, 15 min, quenched	*MA1420q*
1000 °C, 8 h	*MA1000*
1000 °C, 1 week	*MA1000w*
1000 °C, 8 h, annealed 940 °C, 50 h	*MA940*
1000 °C, 8 h, annealed 800 °C, 8 h	*MA800*
1000 °C, 8 h, annealed 800 °C, quenched	*MA800q*
1200 °C, 8 h	*SS1200*
1100 °C, 8 h	*SS1100*
1000 °C, 8 h	*SS1000*
1000 °C, 1 week	*SS1000w*

In order to compare the properties of MA-derived ceramics with those of solid-state (denoted as "SS") synthesized ordered ceramics, PSN was also prepared by the two-step 'columbite' method.[13] The processing conditions from the literature[5] were used, where high B-site ordering of PSN ceramic was achieved (ESI†). The microstructures and XRD patterns of SS-derived ceramics are shown in ESI,† Fig. S3 and S4.

For microstructural investigation, the ceramic samples were mounted in epoxy and ground and polished using standard metallographic techniques. For the grain size determination, the ceramics were thermally etched at 900 °C and the microstructure of the ceramics was examined using a field-emission scanning electron microscope (FE-SEM, JSM-7600F JEOL Ltd, Tokyo, Japan) at 10 kV. The porosity and the grain size distribution were evaluated from the digitalized images processed using the Image Tool software (UTHSCSA Image Tool Version 3.00. 2002). The median grain sizes of each ceramic specimen were determined by measuring more than 150 grains and they are expressed as Feret's diameter (d_F). Analytical transmission electron microscopy (TEM) (JEOL JEM 2010 and Cs-probe corrected JEM-ARM 200 CF both equipped with a JEOL EDXS detector) was employed for the study of structure properties at the nanometer and atomic scales. The specimens were prepared by mechanical grinding, dimpling and final Ar-ion milling.

The ceramics were analyzed by XRD under similar conditions as described above for powder analysis. In order to determine the phase composition the ceramics were additionally analysed by XRD using a Bruker D8 advance diffractometer using the $CuK_{\alpha 1}$ radiation. The XRD patterns of the sintered pellets were recorded at 2θ from 15° to 120° using a step of 0.0145° and a dwell time of 262.5 s per step. The refinements of the structure at room temperature were made using the Rietveld analysis of the

patterns using the Jana2006 software.[26] The starting unit cell parameters and atomic positions from a previous Rietveld study made by Perrin *et al.* were used.[14] The measured, calculated, and difference diagrams resulting from the Rietveld refinement of the XRD patterns for *MA1000* ceramics are shown in ESI,† Fig. S5. The atomic positions x, y, and z and thermal factors U_{iso} obtained from the refinement as well as the interatomic distances in the coordination spheres of Pb, Sc/Nb and O are summarized in ESI,† Table S2 and Fig. S5.

Additionally, high-energy XRD measurements were carried out at the beamline 11-ID-C of the Advanced Photon Source (APS) at Argonne National Laboratory, Chicago, U.S.A. The powders were placed in a Kapton® capillary and measured in transmission mode using a slit size of 0.5 mm by 0.5 mm and a wavelength λ of 0.11165 Å. Diffraction patterns were collected for five minutes using a Perkin Elmer detector placed about 2.2 meters from the sample. The use of an area detector provided more solid angle of scattering in order to achieve high counting statistics when integrating the measured data. A cerium dioxide standard was used to calculate the sample to detector distance, beam center, and detector orthogonality for data extraction from the two-dimensional XRD pattern. Using *Fit2D*,[27] two-dimensional XRD patterns were reduced to one-dimensional, intensity *versus* 2θ patterns.

For electric measurements, the surfaces of ~200 μm thick samples were covered by sputtered Cr/Au electrodes with a diameter of 5 mm. The dielectric permittivity (ε) and dielectric losses ($\tan\delta$) were measured during cooling from 200 °C down to room temperature using an HP 4284 A precision LCR meter at frequencies of 1, 10, and 100 kHz. The electrical polarization (P) *vs.* the electric field (E) hysteresis loops were measured using a commercial setup Aix-PES (Aixacct Systems, Aachen, Germany). A bipolar sine wave with a frequency of 1 Hz was used as an input signal.

Results and discussion

The microstructural properties of MA-derived ceramics were uniform and are shown in Fig. 1. The ceramics were highly dense, *i.e.*, about 99% of theoretical density, which is consistent with the measured fraction of porosity (~1%) obtained from microstructural analysis. In Fig. 2 the XRD patterns of the MA-derived PSN ceramics exposed to different thermal treatments are shown where no secondary phases were detected. Rietveld refinements revealed the rhombohedral structure with space group $R3m$ in agreement with ref. 5 and 28. Furthermore, no superstructure peaks were observed for ceramics sintered above or below the previously reported T_{OD} (~1200 °C). The most pronounced superstructure peak ($\frac{1}{2}\ \frac{1}{2}\ \frac{1}{2}$), which, according to ref. 6 and 7, should appear at $2\theta \sim 18^\circ$ is not observed (Fig. 2). This is expected considering that the intensity of this peak is very low even for highly ordered samples[6] and, thus, might not appear due to instrumental limitations. Taking this into account we can understand the absence of superstructure peaks in also the XRD patterns of SS-derived ceramics.

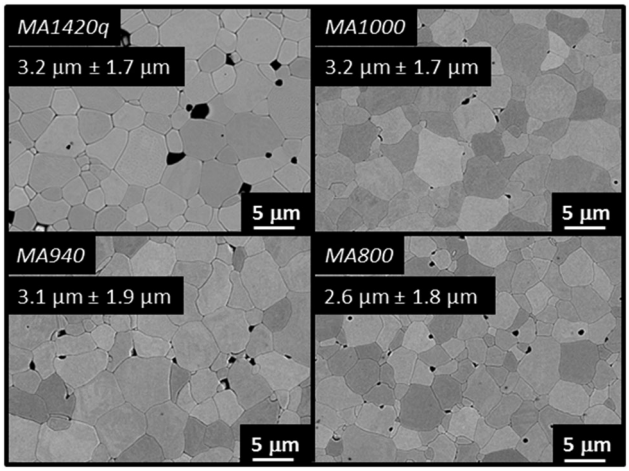

Fig. 1 FE-SEM micrographs of the thermally etched ceramics, prepared as described in Table 1. The median grain size d_F is added for each sample. In the micrograph of the *MA1420q* ceramics some pull-outs are observed due to the polishing procedure.

In the next step, Raman spectroscopy and XRD from the APS were used to determine the ordering degree of PSN ceramics. However, the results from Raman analysis suggested that this technique was insufficient for the determination of the degree of B-site ordering of PSN ceramics (Fig. S6, ESI†). The Raman spectral signature is in fact more strongly influenced by the local defect population, rather than the degree of long-range B-site ordering.[29] Hence, to precisely identify the ordered/disordered character of the materials produced in this work, we relied on XRD measurements conducted at the APS since synchrotron sources typically result in far better resolution than laboratory diffractometers. From the APS XRD measurements, the superstructure peak ($\frac{1}{2}\ \frac{1}{2}\ \frac{1}{2}$) was observed (Fig. 3). In this case, the peak ($\frac{1}{2}\ \frac{1}{2}\ \frac{1}{2}$) is clearly observed in *SS1000* and *SS1000w*, while in *MA1000* and *MA1000w* ceramics only a broad and weak peak profile is observed, suggesting short-range B-site ordering, which we next analyse using STEM.

The ordering degree of Sc^{3+} and Nb^{5+} cations in the *MA1000* ceramics was additionally studied on the atomic level by TEM (Fig. 4). In the TEM dark-field (DF) image of a grain obtained using ($\frac{1}{2}\ \frac{1}{2}\ \frac{1}{2}$) reflection (Fig. 4a), regions with a brighter contrast (labelled with arrows) are seen. A selected area diffraction (SAED) pattern of the grain in the ⟨110⟩ zone axis (inset of Fig. 4a) shows very weak and diffuse ($\frac{1}{2}\ \frac{1}{2}\ \frac{1}{2}$) superstructure reflections along the [111] direction. This type of reflection was previously observed in PSN and it was attributed to the structural ordering of the B-cations, *i.e.*, Sc and Nb.[9,14] The contrast in Fig. 4a indicates that weak local ordering in these regions exists. In order to further understand the chemical ordering of B-cations, an atomically resolved Cs-probe aberration corrected STEM was employed. The B-site intensity profile performed on the high angle annular dark-field scanning transmission electron microscopy (HAADF-STEM) image (Fig. 4b) revealed ordered (O) regions with alternating Nb/Sc intensities among the disordered (D) ones with similar Nb/Sc intensities. The inverse fast Fourier transform (FFT) of the HAADF-STEM

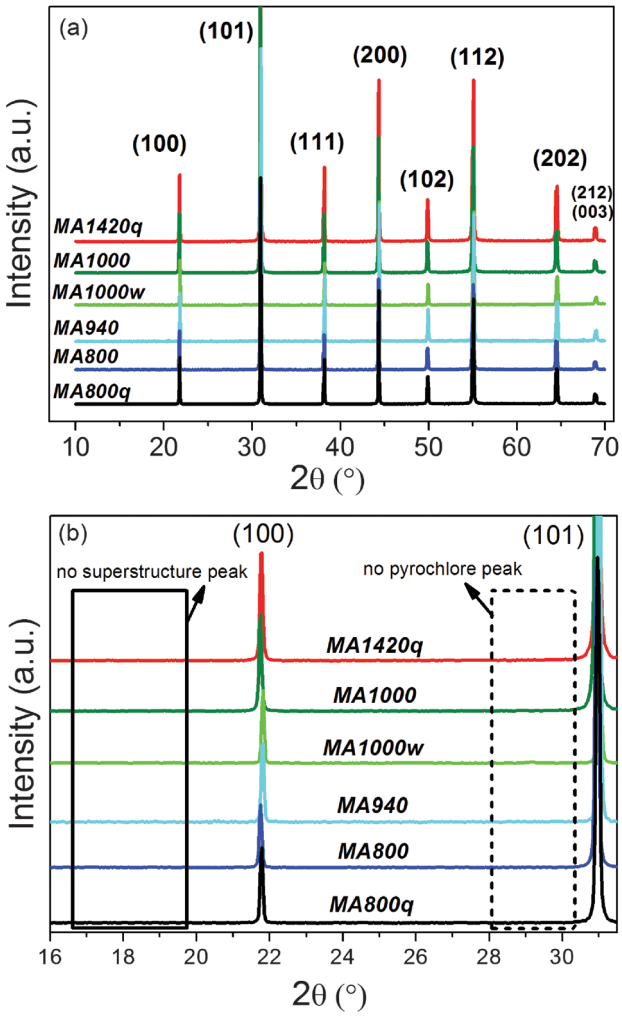

Fig. 2 (a) Room-temperature XRD spectra (PANalytical X'Pert PRO MPD using the Cu-$K_{\alpha 1}$ radiation) of the PSN ceramics exposed to different thermal treatments as described in Table 1. The indexed peaks of the perovskite phase are shown in brackets (ICSD #80922). (b) Zoom of the XRD spectra from 16° to 31.5° showing that there is no secondary-phase (dashed box) or superstructure peaks (solid box).

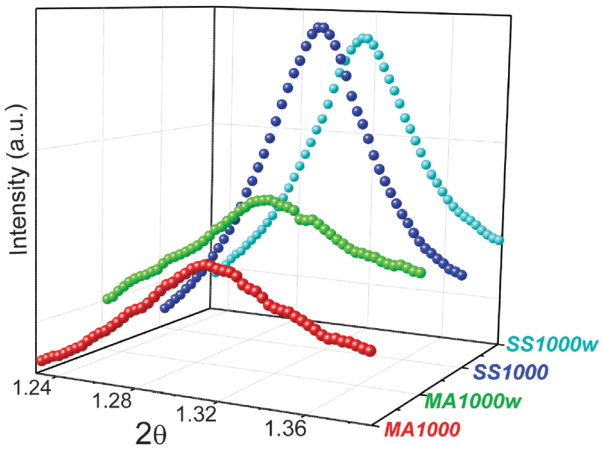

Fig. 3 Synchrotron XRD spectra in the range 2θ from 1.22° to 1.40° carried at beamline 11-ID-C of the advanced photon source. Note that due to the short wavelength of the source (λ = 0.11165 Å) the super-structure peak ($\frac{1}{2}\frac{1}{2}\frac{1}{2}$) appears in the range 2θ from 1.22° to 1.40°.

image (Fig. 4c) shows that these B-site ordered regions are around 2 nm in size.

The TEM data demonstrate the existence of nanometre sized, B-site ordered regions within the grains in *MA1000* ceramics (Fig. 4). These regions are short-range ordered, *i.e.*, they do not extend throughout the entire grain. In contrast, the B-site ordered regions in *SS1000* ceramics are larger and extend over the entire grain. This is shown in Fig. 5. In this case, alternating Nb/Sc ordering is long range and was thus observed over the entire grain (Fig. 5b) with characteristic ($\frac{1}{2}\frac{1}{2}\frac{1}{2}$) reflections and APBs related to the inversion of the sense of the B-site cation ordering (Fig. 5a, c and d).

The TEM data are consistent with the results of the XRD analysis (Fig. 3), in which case a clear superstructure ($\frac{1}{2}\frac{1}{2}\frac{1}{2}$) peak was observed in the *SS1000* sample, whereas only a weak ($\frac{1}{2}\frac{1}{2}\frac{1}{2}$) peak was detected in the *MA1000* sample. This weak and broad XRD peak (Fig. 3) is likely related to short-range B-site ordering in MA-derived ceramics as observed by TEM (Fig. 4). On the other hand, the appearance of antiphase boundaries (AFBs) in *SS1000* ceramics (Fig. 5) indicates that B-site ordering nucleates at different sites within the grain. Depending on the sequence of the B-site ordering (Nb–Sc–Nb or Sc–Nb–Sc) during growth, inversion of the Sc/Nb ordering sequence could form AFBs.

In general, ordering at the B-sites in perovskites requires diffusion of the B-site cations. These cations are slowly diffusing species.[30,31] In relation to the origin of the different B-site ordering in the PSN materials, we may suggest that the diffusion processes in the MA-derived samples are slower in comparison to those in the SS samples. This may be a result of the high level of chemical homogeneity on the nano-scale, which reduces the chemical gradient and thus the driving force for diffusion, and/or due to the presence of crystalline microstrains induced in the material during the mechanochemical activation,[25,32,33] which may freeze the observed disordered state of the Nb and Sc cations.

The ε *vs.* temperature (T) curves were measured for all ceramics and are presented in Table 1. In Fig. 6 ε and $\tan\delta$ *versus* T are shown for selected samples, *i.e.*, for SS-derived ceramics annealed at and below T_{OD} (~1200 °C) and MA-derived ceramics annealed below T_{OD}. It was reported that PSN ceramics sintered at $T > T_{OD}$ displays diffuse relaxor behaviour with a peak in ε at ~110 °C,[5,8] while PSN ceramics sintered at $T < T_{OD}$ exhibits a "classical" ferroelectric behaviour with the peak in ε appearing at a lower temperature (between 80–100 °C[5,9]) and with no relaxation properties.[5] As can be seen in Fig. 6, the ε–T curves of SS-derived ceramics are in agreement with the literature data,[5,8] *i.e.*, the ceramic sintered at T_{OD} displays a diffuse relaxor behaviour with the ε peak of 49 000 at 1 kHz at 107 °C, while the sample sintered at $T < T_{OD}$ shows only a weak relaxation, with a much lower ε peak of 21 000 at 1 kHz and ~95 °C (Fig. 6). This observation is in agreement with the XRD and TEM results where for SS-derived ceramics sintered at $T < T_{OD}$ long range ordered behaviour was observed. The lower ε of *SS1000* ceramic can also be partially related to the smaller

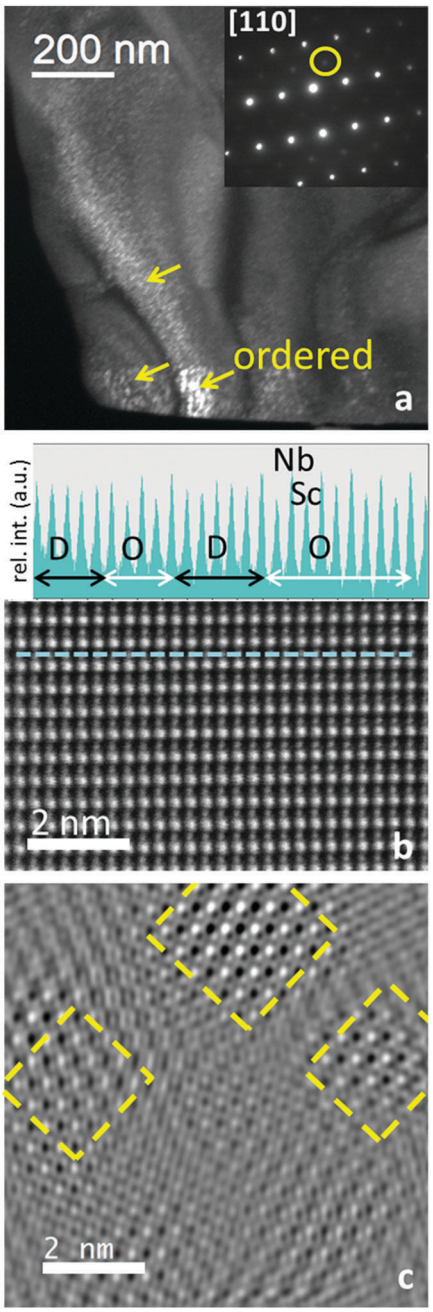

Fig. 4 (a) TEM-DF image of the *MA1000* grain with the corresponding SAED pattern in the [110] zone axis. Ordered areas within the grain are marked with arrows. A weak and diffuse $(\frac{1}{2}\frac{1}{2}\frac{1}{2})$ superstructure reflection is marked with a circle, (b) HAADF-STEM image with the corresponding intensity profile of B site ions (O, and D-ordered/disordered area); the dotted line represents the area where the intensity profile was performed. (c) Inverse FFT image from superstructure reflections with marked B-site ordered areas.

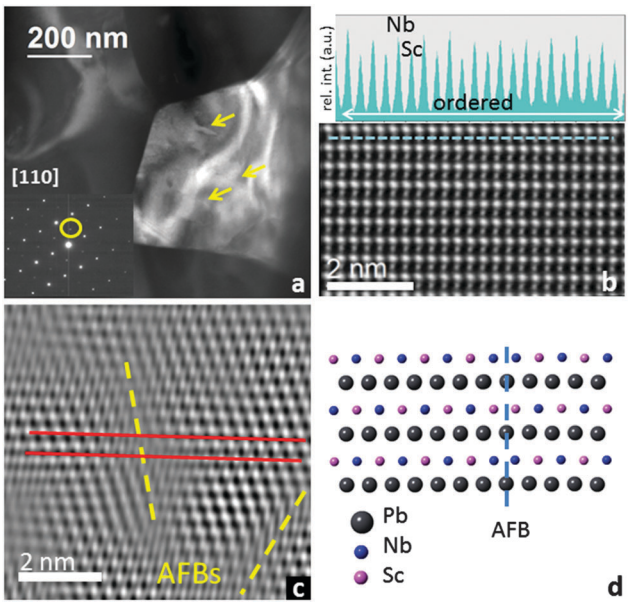

Fig. 5 (a) TEM-DF image of the *SS1000* ceramic grain with the corresponding SAED pattern in the [110] zone axis. Between ordered regions antiphase boundaries (AFBs) were observed (labelled with arrows) as also observed by Perrin *et al.*[9] The superstructure reflection at $(\frac{1}{2}\frac{1}{2}\frac{1}{2})$ is marked with a circle, (b) HAADF-STEM image with the corresponding intensity profile of B site ions, with alternating Nb/Sc intensities. The dotted line represents the area where the intensity profile was performed, (c) inverse FFT image from superstructure reflections with marked AFB. Two red parallel lines indicate the change in B-site contrast intensity, (d) model of the ordered PSN structure showing the AFB.

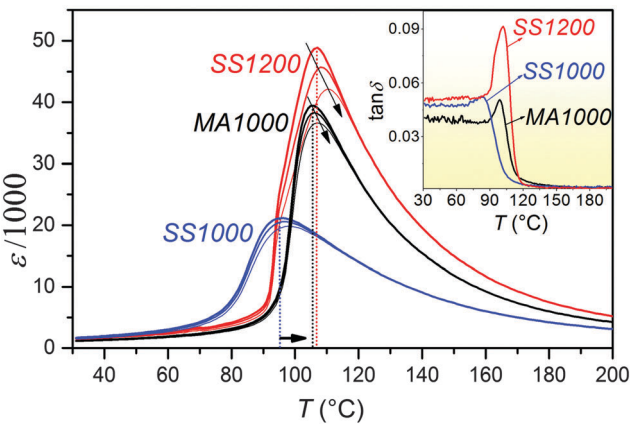

Fig. 6 $\varepsilon - T$ at 1, 10 and 100 kHz and (inset) $\tan\delta$ *vs.* temperature at 10 kHz for *MA1000*, *SS1000* and *SS1200*.

average grain size of this ceramic in comparison to *SS1200* (0.7 μm *vs.* 3.2 μm). Note that for *SS1200* the relaxor to ferroelectric phase transition appears at ~94 °C (see the knee point in Fig. 6), which is in close agreement with the literature.[34,35]

On the other hand, the *MA1000* ceramic annealed below 1200 °C shows diffuse relaxor behaviour with the high ε peak of ~40.000 at 1 kHz at 106 °C (Fig. 6). In addition to this peak, a sharp drop of the permittivity at ~97 °C indicates a relaxor-to-ferroelectric phase transition. For more details regarding this phase transition at ~97 °C, we refer to the complete analysis of the dielectric properties of *MA1000* ceramics reported in our previous study.[36] Note that in PSN single crystals the relaxor-to-ferroelectric phase transition was also observed at ~97 °C.[34,35] Similar ε–T behaviour was obtained for all MA-derived samples from Table 1. Hence, the ε–T measurements indicate the long-range disordered

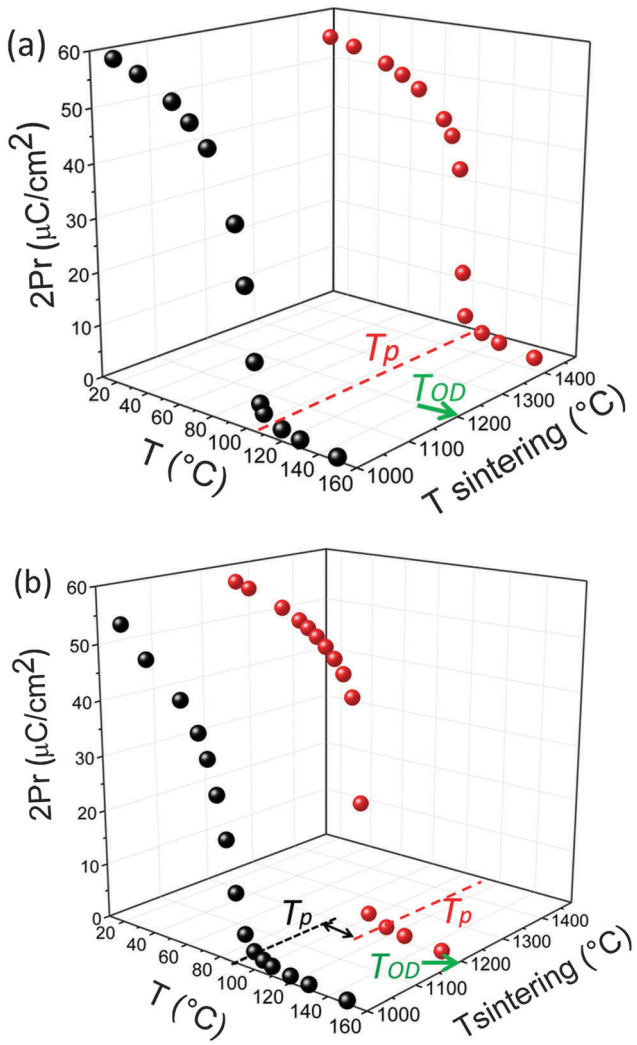

Fig. 7 Temperature dependence of $2P_r$ for (a) *MA1000*, and *MA1420q* and (b) *SS1000*, and *SS1200*. The sintering temperature of ceramics is shown in the *y* axis. The T_{OD} value from the literature[3,4] is marked by an arrow. In (a) the dashed horizontal lines represent the T_p value of *MA1000* and *MA1420q* ceramics. In (b) the red dashed horizontal line represents the T_p value for *SS1200*. The dark dotted horizontal line represents the T_p value for *SS1000*. The black arrow marks the difference of ~20 °C between these two temperatures.

behaviour of MA-derived ceramics even if sintered at 1000 °C, which is ~200 °C below T_{OD}. These findings are in accordance with bulk disorder including only nanometre-sized ordered regions observed by TEM and indirectly by XRD. $\tan\delta$ *vs.* *T* shows a similar trend (inset in Fig. 6). *SS1200* and *MA1000* display a peak in $\tan\delta$ above 100 °C, while the *SS1000* ceramic displays it at a much lower temperature of ~85 °C. The lowest $\tan\delta$ for the majority of the measurement range is observed for MA-derived ceramics.

Furthermore, the *P*–*E* hysteresis loops *vs.* *T* for the MA-derived ceramics are well saturated at 25 °C and reveal the ferroelectric behaviour of the ceramics (Fig. S7 in the ESI†). The remnant polarization (P_r) and the coercive field (E_c) at 25 °C and 1 Hz are 31 μC cm^{-2} and 5 kV cm^{-1}, respectively. Note that the P_r value is higher[10,37] or comparable[4] than the previously reported data measured at room temperature for the disordered PSN. A possible reason for the large polarization of the PSN ceramics prepared in this work could be related to the displacement of the B-site cations, which is much higher than the reported values, namely 1.95 Å/2.13 Å as compared to 2.02 Å/2.06 Å.[5] Note that in ref. 4 the structural data are not given and hence the full comparison cannot be made.

In order to further understand the B-site ordering in MA-derived PSN ceramics, temperature dependence of P_r *vs.* *T* was investigated and is shown in Fig. 7(a) for selected samples. It was reported[4] that in a disordered PSN ceramics the temperature at which the $2P_r$ value sharply drops almost to zero (T_p) is observed above 100 °C (until ~106 °C), which is in agreement with our measurements where T_p is ~105 °C. Similar behaviour was obtained for all MA-derived ceramics (Table 1). This was confirmed also by Raman spectroscopy by tracking the disappearance of a soft mode in all compositions. Hence, in MA-derived ceramics the T_p value is similar regardless of thermal treatment shown in Table 1 (Fig. 7(a), red horizontal line). These results again indicate the long-range disordered behaviour of MA-derived ceramics sintered at 1000 °C, which is in agreement with the results of XRD, TEM and dielectric spectroscopy analyses. In contrast, for SS-derived samples T_p differs with the sintering temperature (Fig. 7(b)). For samples sintered at $T < T_{OD}$, T_p is as low as ~90 °C, while for *SS1200* ceramic T_p appears at ~110 °C, which is in agreement with the literature[4] for ordered (and partially ordered) and disordered ceramics, respectively. Hence, from XRD and TEM analyses, dielectric spectroscopy and $2P_r$ *vs.* *T* measurements, it can be concluded that the MA-ceramics (Table 1) exhibits the long-range disorder behaviour of B-site cations.

Conclusions

PSN ceramics prepared from the mechanochemically activated powder and sintered 200 °C below T_{OD} exhibited behaviour consistent with long-range disorder of the B-site cations. This is in contrast to the behaviour of PSN ceramics prepared by conventional solid-state synthesis. Through different ordering of B-site cations in PSN, the processing route has a marked effect on the dielectric properties and polarization of the material. By comparing the mechanochemically derived and solid-state-derived ceramics sintered at 1000 °C, we showed that the dielectric permittivity in the vicinity of the phase transition to the non-polar phase of the MA ceramics is higher than that of the SS ceramics. Furthermore, the remnant polarization of the MA ceramics sharply drops to almost zero at temperatures higher than 105 °C, in contrast to the SS samples, where this occurs below 15 °C. The different B-site ordering behaviour and the associated properties of the two PSN ceramics might be attributed to a different level of nano-scale chemical homogeneity and/or crystalline microstrains.

The results of this work have established an understanding of the relationship between the synthesis method for PSN ceramics,

B-site cation ordering in the ceramics, and their functional properties. Additionally, this work provided a critical re-examination of the ordered–disordered behaviour of PSN ceramics particularly in relation to the processing.

Acknowledgements

Technical support by J. Cilenšek, B. Kmet, D. Žehelj, K. Kuhar and B. Tratnik from JSI is gratefully acknowledged. The authors thank the Slovenian Research Agency for the financial support (programs P2-0105, P1-0125 and bilateral project BI-US/15-16-60). This research used resources of the Advanced Photon Source, a U.S. Department of Energy (DOE) Office of Science User Facility operated for the DOE Office of Science by Argonne National Laboratory under Contract no. DE-AC02-06CH11357. Jones and Esteves gratefully acknowledge support of this research from the U.S. National Science Foundation (DMR-1409399).

Notes and references

1 G. King and P. M. Woodward, *J. Mater. Chem.*, 2010, **20**, 5785.
2 P. Baettig and N. A. Spaldin, *Appl. Phys. Lett.*, 2005, **86**, 012505.
3 C. G. F. Stenger and A. J. Burggraaf, *Phys. Status Solidi A*, 1980, **61**, 275.
4 C. G. F. Stenger and A. J. Burggraaf, *Phys. Status Solidi A*, 1980, **61**, 653.
5 C. Malibert, B. Dkhil, J. M. Kiat, D. Durand, J. F. Berar and A. Spasojevic-de Bire, *J. Phys.: Condens. Matter*, 1997, **9**, 7485.
6 M. Zhu, C. Chen, J. Tang, Y. Hou, H. Wang, H. Yan, W. Zhang, J. Chen and W. Zhang, *J. Appl. Phys.*, 2008, **103**, 084124.
7 L. Farber, M. Valant, M. A. Akbas and P. K. Davies, *J. Am. Ceram. Soc.*, 2002, **85**, 2319.
8 F. Chu, I. M. Reaney and N. Setter, *J. Appl. Phys.*, 1995, **77**, 1671.
9 C. Perrin, N. Menguy, O. Bidault, C. Y. Zahra, A. M. Zahra, C. Caranoni, B. Hilczer and A. Stepanov, *J. Phys.: Condens. Matter*, 2001, **13**, 10231.
10 N. Yasuda and K. Fujita, *Ferroelectrics*, 1990, **106**, 275.
11 M. Szafranski, A. Hilczer and W. Nawrocik, *J. Phys.: Condens. Matter*, 2004, **16**, 7025.
12 A. A. Bokov, I. P. Raevskii, V. G. Smotrakov and S. M. Zaitsev, *Crystallogr. Rep.*, 1987, **32**, 769.
13 S. L. Swartz and T. R. Shrout, *Mater. Res. Bull.*, 1982, **17**, 1245.
14 C. Perrin, N. Menguy, E. Suard, C. Muller, C. Caranoni and A. Stepanov, *J. Phys.: Condens. Matter*, 2000, **12**, 7523.
15 D. Kuščer, A. Meden, J. Holc and M. Kosec, *J. Am. Ceram. Soc.*, 2006, **89**, 3081.
16 J. Xue, J. Wang and T. M. Rao, *J. Am. Ceram. Soc.*, 2001, **84**, 660.
17 X. S. Gao, J. M. Xue, J. Wang, T. Yu and Z. X. Shen, *Appl. Phys. Lett.*, 2003, **82**, 4773.
18 J. Wang, D. M. Wan, J. M. Xue and W. B. Ng, *Adv. Mater.*, 1999, **11**, 210.
19 D. Kuščer, J. Holc and M. Kosec, *J. Am. Ceram. Soc.*, 2007, **90**, 29.
20 M. Kosec, H. Uršič, J. Holc, M. Hrovat, D. Kuščer and B. Malič, *IEEE Trans. Sonics Ultrason.*, 2010, **57**, 2205.
21 M. Alguero, A. Moure, L. Pardo, J. Holc and M. Kosec, *Acta Mater.*, 2006, **54**, 501.
22 H. Uršič, J. Tellier, J. Holc, S. Drnovšek and M. Kosec, *J. Eur. Ceram. Soc.*, 2012, **32**, 449.
23 H. Uršič, J. Holc and M. Kosec, *J. Eur. Ceram. Soc.*, 2013, **33**, 795.
24 M. Alguero, J. Ricote and A. Castro, *J. Am. Ceram. Soc.*, 2004, **87**, 772.
25 T. Rojac, A. Benčan, H. Uršič, B. Malič and M. Kosec, *J. Am. Ceram. Soc.*, 2008, **91**, 3789.
26 V. Petricek, M. Dusek and L. Palatinus, *Jana2006. The crystallographic computing system*, Institute of Physics, Praha, Czech Republic, 2006.
27 A. P. Hammersley, FIT2D: An Introduction and Overview. ESRF Intern. Rep. ESRF91HA02, 1997.
28 K. S. Knight and K. Z. Baba-Kishi, *Ferroelectrics*, 1995, **173**, 341.
29 B. Mihailova, M. Gospodinov, B. Guttler, D. Petrova, R. Stosch and U. Bismayer, *J. Phys.: Condens. Matter*, 2007, **19**, 246220.
30 B. Malič, D. Jenko, J. Holc, M. Hrovat and M. Kosec, *J. Am. Ceram. Soc.*, 2008, **91**, 1916.
31 M. V. Slinkina and G. I. Doncov, *Neorg. Mater.*, 1992, **28**, 567.
32 M. Alguero, J. Ricote, T. Hungria and A. Castro, *Chem. Mater.*, 2007, **19**, 4982.
33 M. Alguero, P. Ramos, R. Jimenez, H. Amorin, E. Vila and A. Castro, *Acta Mater.*, 2012, **60**, 1174.
34 Y. H. Bing and Z. G. Ye, Piezo- and ferroelectric (1-x)Pb(Sc1/2Nb1/2)O3-xPbTiO3 solid solution system, in *Handbook of advanced dielectric, piezoelectric and ferroelectric materials*, ed. Z. G. Ye, Woodhead Publishing Limited, Cambridge, 2008.
35 Y. H. Bing, A. A. Bokov and Z. G. Ye, *Curr. Appl. Phys.*, 2011, **11**, S14.
36 V. Bobnar, H. Uršič, G. Casar and S. Drnovšek, *Phys. Status Solidi B*, 2013, **250**, 2232.
37 F. Kuchar and M. W. Valenta, *Phys. Status Solidi*, 1971, **6**, 525.